Quaternary International 462 (2017) 124–129

Contents lists available at ScienceDirect

Quaternary International

journal homepage: www.elsevier.com/locate/quaint

Continuous GPS measurements of crustal deformation in Garhwal-Kumaun Himalaya

Param K. Gautam [a, *], V.K. Gahalaut [b], Sanjay K. Prajapati [b], Naresh Kumar [a], Rajeev K. Yadav [c], Naresh Rana [b], Chandra P. Dabral [a]

[a] Wadia Institute of Himalayan Geology, Dehradun, India
[b] National Centre for Seismology, Ministry of Earth Sciences, New Delhi, India
[c] CSIR-National Geophysical Research Institute, Hyderabad, India

ARTICLE INFO

Article history:
Received 5 June 2016
Received in revised form
22 May 2017
Accepted 24 May 2017
Available online 5 June 2017

Keywords:
GPS
Crustal deformation
Himalaya

ABSTRACT

We report GPS measurements of crustal deformation from five continuous sites in the Garhwal Kumaun Himalaya. The motion at these sites confirms strain accumulation on the Main Himalayan Thrust (MHT) under the Outer and Lesser Himalaya with a slip deficit rate of 18 mm/year over a width of ~100 km. Apart from secular plate motion, these sites also exhibit seasonal variations. We model these seasonal variations using the global models of atmospheric and hydrological loads. The influence of these loads is maximum in the vertical component which decreases in the north and then in the east component. All the four sites in the Himalayan region and a site at Delhi show consistency between the observed seasonal variations with that predicted by the model. However, the annual variations in the horizontal component of displacement time series at BDRI (Badrinath) GPS site are not consistent with the predictions which could be due to local site conditions.

1. Introduction

Convergence across the Himalayan arc occurs through stick and slip manner on the Main Himalayan Thrust (MHT) that lies under the Outer and Lesser Himalaya. The MHT further north under the Higher and Tethys Himalaya slips aseismically. The two distinct parts of the MHT are connected through the ramp which forms the transition from seismically active MHT in the updip side to the aseismically slipping MHT that lies downdip of the ramp (e.g., Caldwell et al., 2013; Stevens and Avouac, 2015; Bilham et al., 2017). This transition zone is also marked by the small and moderate magnitude thrust earthquakes of the Himalayan seismic belt. So strain accumulation on the seismically active MHT under the Outer and Lesser Himalaya occurs in the interseismic period, to be released coseismically during M > 7 earthquakes. This has amply been demonstrated by the GPS measurements in various parts of the Himalayan arc (Banerjee and Bürgmann, 2002; Banerjee et al., 2008; Ponraj et al., 2010; Khandelwal et al., 2014; Jade et al., 2014). Extensive GPS measurements in Nepal show evidence of strain accumulation on the Main Himalayan Thrust (MHT) at a rate corresponding to ~20 mm/year (e.g., Bilham et al., 1997; Jouanne et al., 1999; Avouac, 2003; Bettinelli et al., 2008; Ader et al., 2012). In the source zone of the 2015 Gorkha earthquake, entire accumulated strain, or some part of it, was released coseismically during the earthquake (Avouac et al., 2015). Indeed, that region showed evidence of strain accumulation in the preceding years.

The Garhwal Kumaun region of NW Himalaya has not experienced a great earthquake in past few hundred years. The 1905 Kangra earthquake rupture (M 7.8) did not extend up to this region, though Middlemiss (1910) reported damage in the Dehradun region. Recent damaging earthquakes, the 1991 Uttarkashi and 1999 Chamoli, were of strong magnitude and their ruptures were confined close to the downdip part of the seismically active MHT. Thus these earthquakes too did not release any substantial strain on the MHT that must have accumulated over the preceding years. Here, in this article, we report continuous GPS measurements of crustal deformation from five sites which show evidence of strain accumulation in the Garhwal Kumaun Himalaya. We also show seasonal variation in the displacement time series, its spatial and temporal variation.

* Corresponding author.
E-mail address: param@wihg.res.in (P.K. Gautam).

http://dx.doi.org/10.1016/j.quaint.2017.05.043
1040-6182/

2. Continuous GPS measurements in Garhwal Kumaun region

In the Garhwal Kumaun Himalayan region, five continuous GPS sites (Fig. 1) have been installed. Many of these sites (GHUT, WIHG, BDRI and MUNS) are operating since 2007. In addition to the sites in the Garhwal Kumaun region, a continuous GPS site at Delhi has been established and is in operation since 2010. All these sites are located on concrete pillar established on hard rock. However, the site at Dehradun is located on roof top of a two storey building. In case hard rock is not available the pillar extends upto a depth of 4–5 feet below ground to reach to the firm ground. Continuous GPS data from these sites have been analysed together with several IGS sites surrounding the Indian plate, namely, IISC, LHAZ, GUAO, URUM, CHUM, KUNM, WUHN, SELE, POL2, TEHN, BAHR, DARW, KIT3, HYDE, BHR1, BHR2, LCKI, LCK2, and SOLA. We used GAMIT, version 10.40 (King and Bock, 2006; Herring et al., 2010a, b), to derive the loosely constrained site coordinates. The site position estimates and their rates were estimated in ITRF2008 (Altamimi et al., 2011) by stabilizing more stable continuous sites and core IGS reference sites using GAMIT/GLOBK, GLORG. We have used the GMF (Global Mapping Function) and apriori pressure and temperature from the GPT2 model have been used in absence of in situ meteorological data (Boehm et al., 2006; Lagler et al., 2013). The ocean tide model FES2004 (Letellier, 2004) has been used for the removal of contributions from ocean tidal loads at the site locations. The IERS2003 model has been used for the correction of site displacement associated with solid earth deformation produced by tidal potential (McCarthy and Petit, 2004). In ITRF2008, these sites moves at the rate varying from ~48 mm/year towards N45° (DELI, at Delhi) to ~36 mm/year towards N51°(BDRI, at Badrinath, Table 1). The time series of these sites are available in the accompanying supplementary material (Fig. S1). All the sites, apart from showing the secular plate motion towards northeast, also show annual seasonal variations, which have been discussed in the subsequent section. We estimated the site velocity in Indian reference frame by considering the Indian plate rotation pole of Ader et al. (2012). In Indian reference frame, the velocity at site DELI is less than 2 mm/year, which is as per the expectations, as DELI is located on the Indian plate. All sites show predominantly southward and arc normal velocity which increases towards north (Fig. 1).

3. Seasonal variation

One of the spectacular features of the time series of GPS measurements is the seasonal variations. We remove the secular trend from these sites and show the seasonal variations at these sites (Fig. 2). The most prominent amongst these variations are the annual variations. Although there could be some additional low amplitude high frequency variations present in these measurements, but we ignore them here as the accuracy in GPS measurements and processing, and limited spatial and sparse coverage by our network, do not warrant to take up such an analysis. Annual variations have been reported earlier also (Bettinelli et al., 2008; Bollinger et al., 2007; Khandelwal et al., 2014; Chanard et al., 2014; Flouzat et al., 2009). Bettinelli et al. (2008) proposed that the seasonal variations are due to the recharging/loading of the Indo-Gangetic sediments due to rainfall. However, variations in the ocean tide load, non-tidal ocean load, atmospheric pressure load and snow fall can also deform the surface of the Earth (Petit and Luzum, 2010; Dobslaw et al., 2013; Van Dam and Whar, 1987; Heki, 2001). Contribution from the ocean tidal load in the Himalaya is small and has been taken care during the processing of GPS data

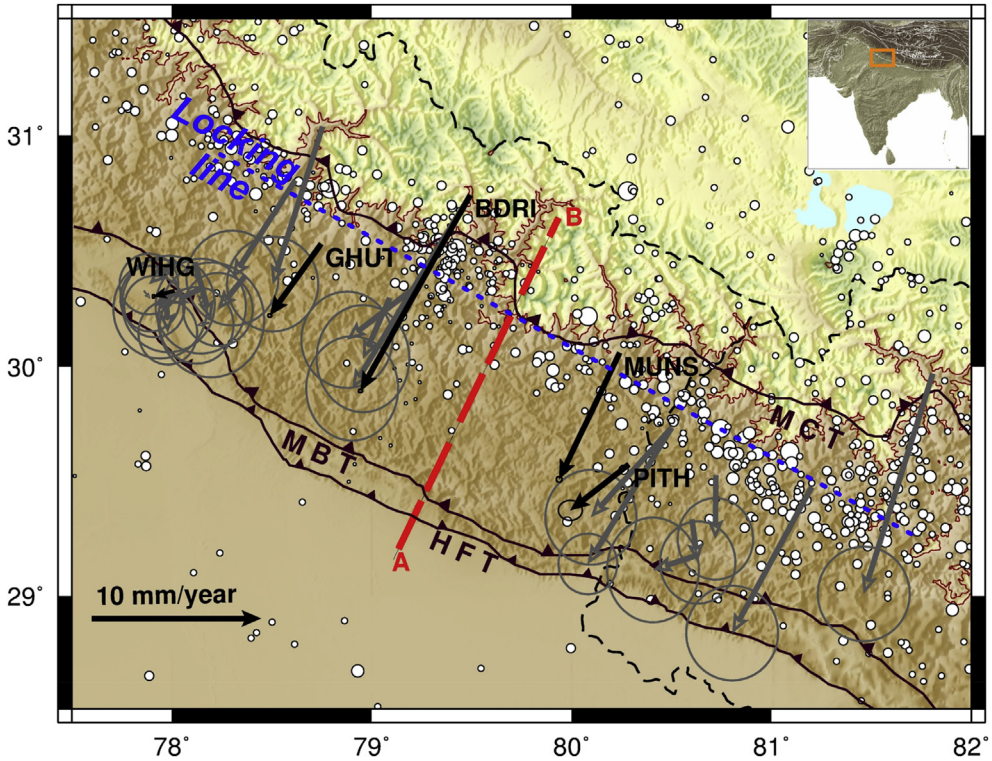

Fig. 1. Site velocity at 5 sites (black arrows) in Indian reference frame. Site velocity from campaign mode studies (grey arrows from Banerjee and Bürgmann, 2002) are also shown. Circles (filled white) are the earthquake epicentres from ISC catalogue during the period 1970–2015. Site motions at a few sites in far western Nepal are also shown. All the measurements are projected along profile AB for analysis of Fig. 3. HFT- Himalayan Frontal Thrust, MBT- Main Boundary Thrust, MCT- Main Central Thrust. Blue dotted line shows the location of locking nine, estimated from this study. (For interpretation of the references to colour in this figure legend, the reader is referred to the web version of this article.)

Table 1
GPS sites used in analysis and their velocities in ITRF2008 and India fixed with associated errors.

Site Code	Longitude (°E)	Latitude (°N)	ITRF 2008 Velocity (mm/year)		India fixed Velocity (mm/year)		Corr
			$V_N \pm 1\sigma$	$V_E \pm 1\sigma$	V_N	V_E	
DELI	77.12	28.48	34.04 ± 0.05	34.25 ± 0.06	1.37	−1.35	0.05
WIHG	78.01	30.32	33.97 ± 0.02	33.31 ± 0.02	1.19	−1.64	0.03
PITH	80.28	29.57	31.83 ± 0.24	32.13 ± 0.26	−1.19	−3.83	0.11
GHUT	78.74	30.53	30.17 ± 0.02	31.64 ± 0.03	−2.69	−3.43	0.05
MUNS	80.24	30.06	27.04 ± 0.07	31.77 ± 0.07	−5.98	−3.95	0.04
BDRI	79.49	30.74	22.90 ± 0.03	28.30 ± 0.03	−10.04	−6.88	0.07

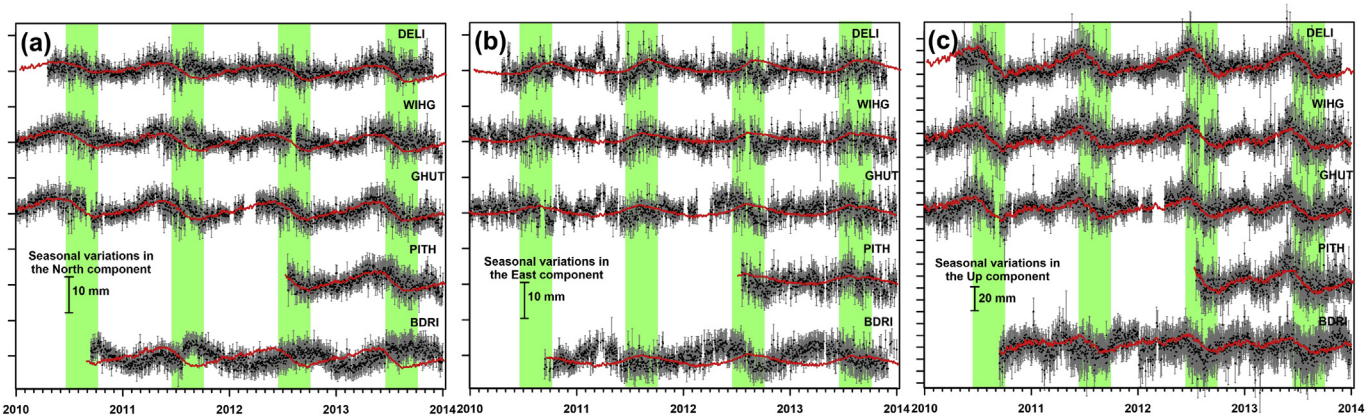

Fig. 2. Seasonal variation at four sites in the Himalayan region along with a site at Delhi (DELI). Scale in each case is indicated. Red curve in each case is the prediction of global hydrological and atmospheric model. The fitting is generally good at all sites except Badrinath (BDRI) where the north and east components are almost in opposite phase with the prediction for east and north components. The green strip in each panel denote the rainy season. The time series at MUNS is not shown because of several breaks, caused by lack of data, in the time series. (For interpretation of the references to colour in this figure legend, the reader is referred to the web version of this article.)

using ocean tide model FES2004 (Letellier, 2004). We have used the global models of atmospheric and hydrological loads and have calculated variations in the north, east and up components of the GPS time series at all sites. Farrell (1972) provided Green's functions which describe the response of an elastic earth to a point load on its surface. Radial and horizontal displacement at any point on the surface of the earth can be estimated by evaluating a convolution between the Green's functions and load functions. Horizontal changes in the atmospheric mass are governed by the pressure loading at the surface and the gravitational attraction of the atmospheric masses and these variations in the horizontal distribution of atmospheric masses induce deformation within the earth (Van Dam and Wahr, 1987). We have used the data and programs provided by the Global Geophysical Fluid Center (GGFC) (Van Dam and Wahr, 1987; Van Dam, 2010, http://geophy.uni.lu/ggfc-atmosphere/ncep-loading.html) for the estimation of surface displacement at a GPS site due to the atmospheric pressure loading. The GGFC provides 6-hourly, global surface displacements at 2.5° × 2.5° derived from the National Center for Environmental Protection (NCEP) reanalysis surface pressure. Further, for the estimation of surface displacement at a GPS site due to the hydrological load, we have used the data and program provided by the GFZ (ftp://ig2-dmz.gfz-potsdam.de/LOADING/HYDL). The hydrological load is taken from the hydrological Land Surface Discharge Model (LSDM) which includes soil moisture, snow and surface water mass in rivers and lakes on a regular grid 0.5° × 0.5° with 1 day time increment (Dill, 2008; Dill and Dobslaw, 2013). Hydrological induced elastic surface deformations are calculated by convolving Farrell's loading Green's function with modelled hydrological mass distributions from the global hydrological model LSDM. Global solution for surface deformation due to non-tidal ocean load at regular grid 0.5° × 0.5° provided by the GeoForschingZentrum (GFZ) using Ocean Model for Circulation and Tides (OMCT) model (ftp://ig2-dmz.gfz-potsdam.de/LOADING/NTOL/) has been taken to estimate the contribution due ocean water mass redistribution (Dobslaw et al., 2013). However, the contribution is insignificant, being only >1 mm in the vertical and >0.5 mm in the horizontal. We have used the elastic deformation using spherical earth model and have computed in the centre of Earth's frame (cF) on the basis of load love numbers given for the elastic Earth model “ak135”.

Predictions at each site are shown in Fig. 2 with red curve. Contributions from the individual loads at each site is shown in Fig. S2. As expected the variations are maximum in up component and the magnitude of variations decreases at sites located northward. The fit between the observed variations and predicted by the model is quite spectacular. Amongst the two horizontal components, the variations in the north component are more prominent. This is expected as in the context of Himalaya, the atmospheric and hydrological loads act as a 2-D load aligned in the east-west direction, causing no or little variations at sites in the east-west direction. However, because of load variation in the north-south direction, there will be corresponding variations in the north component. Earlier, it has been seen that seasonal variations at most of the sites in the Nepal Himalaya is generally consistent with this (Bettinelli et al., 2008; Bollinger et al., 2007; Flouzat et al., 2009). However, at a few sites in Nepal there is a mismatch with the magnitude of variations, the variations at site being large as compared to the prediction. Similarly, there is mismatch in the phase of seasonal variations. In our case, the magnitude of variations at all sites in all components matches with the predicted variation, within the corresponding uncertainties in the

observations. However, there is a mismatch in the phase in the north and east components at site BDRI. There could be two reasons for this. It is possible that the local site conditions are not accounted in the hydrological load computations which is taken over an area of 0.5° × 0.5°. We acknowledge that calculations of atmospheric load is done over 2.5° × 2.5° but it is known that contribution from atmospheric load is minimal. The other possibility for the mismatch in phase could be because of some additional process, other than hydrological and atmospheric load, responsible for it, which could be site specific. Similar mismatch can also be seen at some of the sites in Nepal (Fig. 4a and b of Fu et al., 2013). At this stage, it is difficult to identify the exact process responsible for seasonal variations.

4. Evidence of strain accumulation

The gradual increase in the southward secular velocity from south to north at all sites implies strain accumulation. We use the Okada's formulation (Okada, 1992) of elastic dislocation which provides surface displacements due to slip across a fault in an elastic half space. We assume that the MHT beneath the Himalayan arc is locked. We use a deep slip model in which it is assumed that while the shallow MHT is locked, the deeper part of the MHT slips aseismically and its response can be simulated by assuming a dislocation. Considering that we have only five sites in the Garhwal Kumaun Himalayan region, in our 2D analysis we assumed that the locking on the MHT is uniform and perfect along its entire width. With more data one can consider variation in locking along the MHT (Stevens and Avouac, 2015). We perform a grid search to estimate the dip, updip edge of the aseismically slipping MHT, and slip rate across the MHT. The deeper part of the aseismically slipping MHT is assumed to be extending infinitely northward from the Higher Himalaya. This simulates the steady motion on it. In this model, the updip edge of the aseismically slipping MHT joins with the downdip edge of the locked MHT and is referred as the locking line. By assuming that the MHT extends right up to the Himalayan Frontal Thrust (HFT) and the strain accumulation rate or locking is uniform on the shallow part of the MHT, these estimates effectively provides us width of the locked zone and the slip deficit rate. We estimate them as 95 ± 5 km and 18 ± 2 mm/year, respectively (Fig. 3). To derive these estimate we have considered the available campaign mode GPS measurements from the region (Banerjee et al., 2008) also. The available campaign mode observations were first converted from ITRF2002 to ITRF2008 and then to the Indian reference frame. Their inclusion improved the reliability of the analysis as our measurements are only from 5 sites. The estimate of locked width of the MHT implies that the MHT under the Outer and Lesser Himalaya locked and is accumulating strain at the arc normal rate of 18 ± 2 mm/year.

The rate of plate convergence and also strain accumulation varies along the arc. In the Kashmir region, is about 12–13 mm/year (Schiffman et al., 2013; Kundu et al., 2014) while in the Nepal region, it is 18–20 mm/year (Bilham et al., 1997; Jouanne et al., 1999; Stevens and Avoauc, 2015; Bettinelli et al., 2008; Vernant et al., 2014). Although, the rate is not well constrained in the Eastern Himalaya, it is about 21 mm/year. These rates derived from GPS measurements are consistent with that from the geological studies (Thakur, 2013). In the Garhwal-Kumaun Himalayan region, the rate of strain accumulation is consistent with the earlier estimates (Banerjee et al., 2008; Khandelwal et al., 2014; Jade et al., 2014) and with the estimate obtained from the neighbouring western Nepal region (Stevens and Avouac, 2015). Width of the locked zone is also consistent with the earlier estimates. It has been noticed that the earthquakes of Himalayan seismic belt, and the 3.5 km topography

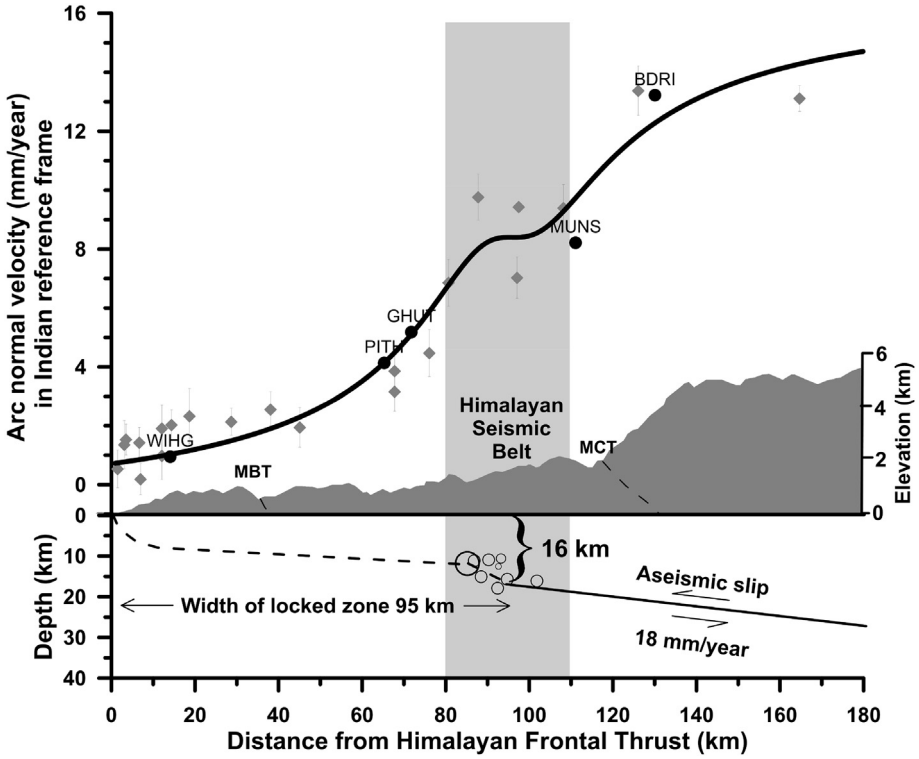

Fig. 3. Arc normal site velocity along a composite profile in the direction along N30°. The continuous curve simulates the effect of locking of a 95 km wide Main Himalayan Thrust (MHT) under the Outer and Lesser Himalaya. The slip deficit rate at the MHT is 18 mm/year. Grey diamonds denote the campaign mode GPS sites of Banerjee and Bürgmann (2002). To avoid cluttering, we have not shown the site names.

contour approximately coincides with the locking line (Cattin and Avouac, 2000). In our case too, the locking line coincides with the Himalayan earthquake belt and the topographic front with topography contour of 3.5 km.

5. Status of strain accumulation

It is assumed that the rate of long term convergence is generally equal to the slip deficit rate as only less than 10% of this rate contributes to permanent deformation (Avouac, 2003) and the rest of the deformation is considered as recoverable. The occurrence of small and moderate earthquakes of the Himalayan seismic belt do not contribute much towards the convergence. Further, it is assumed that slip rates across the plate boundaries are stationary over the periods of hundred to thousand years. In the Garhwal Kumaun region, the last great earthquake probably occurred in 1505. Rajendran et al. (2015) suggested that the 1505 earthquake did not affect this region and they suggested that the last earthquake in this region was probably in thirteenth century. This is also supported by Jayangondaperumal et al. (2017) who suggested an earthquake in 1344 CE. If the current rate of strain accumulation applies over past 700 or even 500 years, then sufficient slip deficit (~10 m, corresponding to a strain of 10^{-4} over 100 km wide zone) has accumulated in the region to be released in a great earthquake.

6. Conclusion

Analysis of continuous GPS measurements from Garhwal Kumaun Himalaya provide evidence for active deformation and strain accumulation for future great and major earthquake in the region. These measurements are consistent with the locking of underlying Main Himalayan Thrust (MHT), from the Himalayan front up to a distance of 95 km across the Himalayan arc. The strain accumulation in this region is occurring corresponding to a slip deficit rate of 18 mm/year. Other than the evidence of strain accumulation, these measurements also show seasonal variations, which are largely caused by the atmospheric and hydrological variations. However, there seems to be some other factors contributing these variability, which need to be explored with more measurements.

Acknowledgements

The authors thank Directors, WIHG, Dehradun and NGRI, Hyderabad for their support and permission to carry out the collaborative work and also acknowledge the coordinators Dr. Sushil Kumar, WIHG and Dr. V.M. Tiwari, NGRI of this collaborative project. We are thankful to Ministry of Earth Sciences, Government of India (MoES/PO(Seismo)/1(256)/2015) for sponsoring MPGO-EPR project and the staffs of the project is thanked for data collection. Comments from the three anonymous reviewers were very constructive.

Appendix A. Supplementary data

Supplementary data related to this article can be found at http://dx.doi.org/10.1016/j.quaint.2017.05.043.

References

Ader, T., Avouac, J.-P., Liu-Zeng, J., Lyon-Caen, H., Bollinger, L., Galetzka, J., Genrich, J., Thomas, M., Chanard, K., Sapkota, S.N., Rajaure, S., Shrestha, P., Ding, L., Flouzat, M., 2012. Convergence rate across the Nepal Himalaya and interseismic coupling on the Main Himalayan Thrust: implications for seismic hazard. J. Geophys. Res. Solid Earth 117, B04403.

Altamimi, Z., Collilieux, X., Metivier, L., 2011. ITRF2008: an improved solution of the international terrestrial reference frame. J. Geodesy 85, 457–473.

Avouac, J.P., 2003. Mountain building, erosion, and the seismic cycle in the Nepal Himalaya. Adv. Geophys. 46, 1–80.

Avouac, J.-P., Meng, L., Wei, S., Wang, T., Ampuero, J.-P., 2015. Lower edge of locked main Himalayan thrust unzipped by the 2015 Gorkha earthquake. Nat. Geosci. 8, 708–711.

Banerjee, P., Bürgmann, R., 2002. Convergence across the northwest Himalaya from GPS measurements. Geophys. Res. Lett. 29, 30–1-30-4.

Banerjee, P., Bürgmann, R., Nagarajan, B., Apel, E., 2008. Intraplate deformation of the Indian subcontinent. Geophys. Res. Lett. 35, L18301.

Bettinelli, P., Avouac, J.P., Flouzat, M., Bollinger, L., Ramillien, G., Rajaure, S., Sapkota, S., 2008. Seasonal variations of seismicity and geodetic strain in the Himalaya induced by surface hydrology. Earth Planet. Sci. Lett. 266, 332–344.

Bilham, R., Larson, K., Freymueller, J., 1997. GPS measurements of present-day convergence across the Nepal Himalaya. Nature 386, 61–64.

Bilham, R., Mencin, David, Bendick, Rebecca, Bürgmann, Roland, 2017. Implications for elastic energy storage in the Himalaya from the Gorkha 2015 earthquake and other incomplete ruptures of the Main Himalayan Thrust. Quat. Int. http://dx.doi.org/10.1016/j.quaint.2016.09.055.

Boehm, J., Niell, A., Tregoning, P., Schuh, H., 2006. Global Mapping Function (GMF): a new empirical mapping function based on numerical weather model data. Geophys. Res. Lett. 33, L07304 http://dx.doi.org/10.1029/2005/GL025546.

Bollinger, L., Perrier, F., Avouac, J.P., Sapkota, S., Gautam, U., Tiwari, D.R., 2007. Seasonal modulation of seismicity in the Himalaya of Nepal. Geophys. Res. Lett. 34, L08304.

Caldwell, W.B., Klemperer, S.L., Lawrence, J.F., Rai, S.S., Ashish, 2013. Characterizing the main Himalayan thrust in the Garhwal Himalaya, India with receiver function CCP stacking. Earth Planet. Sci. Lett. 367, 15–27.

Cattin, R., Avouac, J.P., 2000. Modeling mountain building and the seismic cycle in the Himalya of Nepal. J. Geophys. Res. 105, 13389–13407.

Chanard, K., Avouac, J.P., Ramillien, G., Genrich, J., 2014. Modeling deformation induced by seasonal variations of continental water in the Himalaya region: Sensitivity to Earth elastic structure. J. Geophys. Res. 119, 5097–5113.

Dill, R., 2008. Hydological Model LSDM for Operational Earth Rotation and Gravity Field Variations. Scientific Technical, Report. STR08/09, GFZ Potsdam, Germany, p. 35.

Dill, R., Dobslaw, H., 2013. Numerical simulations of global-scale high-resolution hydrological crustal deformations. J. Geophys. Res. Solid Earth 118, 5008–5017.

Dobslaw, H., Flechtner, F., Bergmann-Wolf, I., Dahle, C., Dill, R., Esselborn, S., Sasgen, I., Thomas, M., 2013. Simulating high-frequency atmosphere-ocean mass variability for dealiasing of satellite gravity observations: AOD1B RL05. J. Geophys. Res. 118 (7), 3704–3711. http://dx.doi.org/10.1002/jgrc.20271.

Farrell, W.E., 1972. Deformation of the Earth by surface loads. Rev. Geophys. 10, 761–797.

Flouzat, M., Bettinelli, P., Willis, P., Avouac, J.P., Héritier, T., Gautam, U., 2009. Investigating tropospheric effects and seasonal position variations in GPS and DORIS time-series from the Nepal Himalaya. Geophys. J. Int. 178, 1246–1259.

Fu, Y., Argus, D.F., Freymueller, J.T., Heflin, M.B., 2013. Horizontal motion in elastic response to seasonal loading of rain water in the Amazon Basin and monsoon water in Southeast Asia observed by GPS and inferred from GRACE. Geophys. Res. Lett. 40, 6048–6053. http://dx.doi.org/10.1002/2013GL058093.

Heki, K., 2001. Seasonal modulation of interseismic strain buildup in Northeastern Japan driven by snow loads. Science 293, 89–92.

Herring, T.A., King, R.W., McClusky, S.C., 2010a. Documentation of the GAMIT GPS Analysis Software Release 10.4. Department of Earth, and Planetary Sciences. Massachusetts Institute of Technology, Cambridge.

Herring, T.A., King, R.W., McClusky, S.C., 2010b. GLOBK, Global Kalman Filter VLBI and GPS Analysis Program, Version 10.4. Department of Earth, and Planetary Sciences. Massachusetts Institute of Technology, Cambridge.

Jade, S., Mukul, M., Gaur, V.K., Kumar, K., Shrungeshwar, T.S., Satyal, G.S., Dumka, R.K., Jagannathan, S., Ananda, M.B., Dileep, K., Banerjee, S., 2014. Contemporary deformation in the Kashmir–Himachal, Garhwal and Kumaon Himalaya: significant insights from 1995–2008 GPS time series. J. Geodesy 88, 539–557.

Jayangondaperumal, R., Daniels, Robyn L., Niemi, Tina M., 2017. A paleoseismic age model for large-magnitude earthquakes on fault segments of the Himalayan Frontal Thrust in the Central Seismic Gap of northern India. Quat. Int. http://dx.doi.org/10.1016/j.quaint.2017.04.008.

Jouanne, F., Mugnier, J.L., Pandey, M.R., Gamond, J.F., Le Fort, P., Serrurier, L., Vigny, C., Avouac, J.P., 1999. Oblique convergence in the Himalayas of western Nepal deduced from preliminary results of GPS measurements. Geophys. Res. Lett. 26, 1933–1936. http://dx.doi.org/10.1029/1999GL900416.

Khandelwal, D.D., Gahalaut, V.K., Kumar, N., Kundu, B., Yadav, R.K., 2014. Seasonal variation in the deformation rate in NW Himalayan region. Nat. Hazard 74, 1853–1861.

King, R.W., Bock, Y., 2006. Documentation of the GAMIT GPS Analysis Software. Massachusetts Institute of Technology, Massachusetts.

Kundu, B., Yadav, R.K., Bali, B.S., Chowdhury, S., Gahalaut, V.K., 2014. Oblique Convergence and Slip Partitioning in the NW Himalaya: Implications from GPS Measurements. Tectonics, p. 33. http://dx.doi.org/10.1002/2014TC003633.

Lagler, Klemens, Schindelegger, Michael, Böhm, Johannes, Krásná, Hana, Nilsson, Tobias, 2013. GPT2: empirical slant delay model for radio space geodetic techniques. Geophys. Res. Lett. 40, 1069–1073.

Letellier, T., 2004. Etude des ondes de maréesur les plateaux continentaux, Thése-doctorale. Université de Toulouse III, p. 237.

IERS Tech. Note 32. In: McCarthy, D.D., Petit, G. (Eds.), 2004. IERS Conventions (2003). Verl. desBundesamtes fur Kartogr. und Geod, Frankfurt am Main, Germany.
Middlemiss, C.S., 1910. The Kangra earthquake of 4 April 1905. Mem. Geol. Surv. India 38, 405.
Okada, Y., 1992. Internal deformation due to shear and tensile faults in a half-space. Bull. Seismol. Soc. Am. 82, 1018–1040.
Ponraj, M., Miura, S., Reddy, C.D., Prajapati, S.K., Amirtharaj, Mahajan, S., 2010. Estimation of strain distribution using GPS measurements in the Kumaun region of Lesser Himalaya. J. Asian Earth Sci. 39, 658–667.
Petit, G., Luzum, B., 2010. IERS Conventions. Federal Office for Cartography and Geodesy, Frankfurt am Main, Germany.
Rajendran, C.P., John, B., Rajendran, K., 2015. Medieval pulse of great earthquakes in the central Himalaya: Viewing past activities on the frontal thrust. J. Geophys. Res. Solid Earth 120. http://dx.doi.org/10.1002/2014JB011015.
Schiffman, C., Bali, B.S., Szeliga, W., Bilham, R., 2013. Seismic slip deficit in the Kashmir Himalaya from GPS observations. Geophys. Res. Lett. 40, 5642–5645. http://dx.doi.org/10.1002/2013GL057700.
Stevens, V.L., Avouac, J.P., 2015. Interseismic coupling of the main Himalayan thrust. Geophys. Res. Lett. 42, 5828–5837.
Thakur, V.C., 2013. Active tectonics of Himalayan frontal fault system. Int. J. Earth Sci. 102 (7), 1791–1810. http://dx.doi.org/10.1007/s00531-013-0891-7.
Van Dam, T.M., Wahr, J.M., 1987. Displacements of the Earth's surface due to atmospheric loading: effects on gravity and baseline measurements. J. Geophys. Res. 92, 1281–1286.
Van Dam, T., 2010. Updated October 2010. NCEP Derived 6-hourly, Global Surface Displacements at 2.5 × 2.5 Degree Spacing.
Vernant, P., Bilham, R., Szeliga, W., Drupka, D., Kalita, S., Bhattacharyya, A., Gaur, V.K., 2014. Clockwise rotation of the Brahmaputra valley: tectonic convergence in the eastern Himalaya, Naga Hills and Shillong plateau. J. Geophys. Res. 119 (8), 6558–6571. http://dx.doi.org/10.1002/2014JB011196.